Relaxation dynamics of modulated magnetic phases in the skyrmion host GaV_4S_8: An ac magnetic susceptibility study

Ádám Butykai,[1,2,*] Sándor Bordács,[1,2] László F. Kiss,[3] Bertalan György Szigeti,[2] Vladimir Tsurkan,[4,5] Alois Loidl,[4] and István Kézsmárki[1,2,4]

[1]*MTA-BME Lendület Magneto-optical Spectroscopy Research Group, 1111 Budapest, Hungary*

[2]*Department of Physics, Budapest University of Technology and Economics 1111 Budapest, Hungary*

[3]*Department of Experimental Solid State Physics, Institute for Solid State Physics and Optics, Wigner-MTA Research Centre for Physics, 1121 Budapest, Hungary*

[4]*Experimental Physics V, Center for Electronic Correlations and Magnetism, University of Augsburg, 86135 Augsburg, Germany*

[5]*Institute of Applied Physics, Academy of Sciences of Moldova, MD 2028, Chisinau, Republic of Moldova*

(Received 16 March 2017; revised manuscript received 25 July 2017; published 22 September 2017)

We report on the slow magnetization dynamics observed upon the magnetic phase transitions of GaV_4S_8, a multiferroic compound featuring a long-ranged cycloidal magnetic order and a Néel-type skyrmion lattice in a relatively broad temperature range below its Curie temperature. The fundamental difference between GaV_4S_8 and the chiral helimagnets, the prototypical skyrmion host compounds, lies within the polar symmetry of GaV_4S_8, promoting a cycloidal instead of a helical magnetic order and rendering the magnetic phase diagram essentially different from that in the cubic helimagnets. Our ac magnetic susceptibility study reveals slow relaxation dynamics at the field-driven phase transitions between the cycloidal, skyrmion lattice and field-polarized states. At each phase boundary, the characteristic relaxation times were found to exhibit a strong temperature dependence, starting from the minute range at low temperatures, decreasing to the micro- to millisecond range at higher temperatures.

DOI: 10.1103/PhysRevB.96.104430

I. INTRODUCTION

Magnetic skyrmions are topologically nontrivial, whirling spin structures, which can form two-dimensional crystals, so-called skyrmion lattices [1,2]. The emergence of the skyrmion lattice phase was identified in the close vicinity of the paramagnetic-helical phase boundary of cubic chiral helimagnets, known as B20 compounds with a $P2_13$ space group [3–7]. Cu_2OSeO_3, belonging to the same space group with a different crystal structure [8] is an insulating material demonstrated to host skyrmions [9,10], with a magnetoelectric character [11–14]. Since their experimental discovery, skyrmions have attracted much attention owing to their potential application as magnetic bits in high-capacity and low-consumption memory devices [15–19].

GaV_4S_8, a member of the lacunar spinel family is an example of skyrmion-host materials with a nonchiral but polar crystal structure [20]. GaV_4S_8 is a semiconductor with a noncentrosymmetric cubic crystal structure at room temperature characterized by the space group $F\bar{4}3m$ and the corresponding T_d point symmetry group. The compound undergoes a cooperative Jahn-Teller distortion at $T_S = 42$ K through the stretching of the lattice along one of the four cubic body diagonals reducing the crystal symmetry to polar rhombohedral, $R3m$ [21–24]. As a result a sizable ferroelectric polarization develops along the rhombohedral axis [25,26]. The depolarization field is reduced by the formation of submicron-sized structural domains of the four possible rhombohedrally distorted variants with the different ⟨111⟩-type rhombohedral axes [21], assembling into an alternating lamellar domain structure [27].

Long-range magnetic ordering arises and thereby the compound becomes a type-I multiferroic at $T_C = 13$ K [25,26,28,29]. The interplay of the symmetric exchange interaction and the antisymmetric Dzyaloshinskii-Moriya (DM) exchange interaction gives rise to a long-wavelength spin ordering. However, in contrast to the B20 compounds featuring a helical spin order in zero field and longitudinal conical spin structure in finite magnetic fields, in GaV_4S_8 the different pattern of DM vectors, dictated by its polar C_{3v} symmetry, leads to a cycloidal spin order (Cyc) and precludes the emergence of the longitudinal conical structure in finite fields [20]. The cycloidal nature of the magnetic modulations has been confirmed experimentally by polarized small-angle neutron scattering (SANS) measurements [30].

In low magnetic fields a Néel-type skyrmion lattice (SkL) develops. Due to the lack of the longitudinal conical state, being the main competitor of the SkL phase in the B20 compounds, the Néel-type SkL is stable over a broad temperature region [20]. On the other hand, the easy-axis anisotropy in the rhombohedral domains [31] promotes the ferromagnetic ordering (FM) of the spins in the ground state, suppressing the modulated phases below $T_F \sim 5$ K even in zero field [20,30]. In the temperature range between $T_F = 5$ K and $T_C = 13$ K moderate magnetic fields drive the modulated structures, Cyc and SkL, to a collinear, field-polarized (FP) state. Since the magnetic easy axis is parallel to the rhombohedral axis, the formation of lamellar structural domain patterns, resulting in the alternation of the anisotropy axes, may influence the magnetic structures, in various aspects:

(i) The modulated (Cyc and SkL) magnetic phases were shown to persist in larger external fields in domains wherein the rhombohedral axis is not parallel to the field, producing a seemingly richer phase diagram in the typically multidomain samples [20]. Owing to the strong easy-axis anisotropy, the

*butykai@mail.bme.hu

critical fields of the phase transitions in each domain are determined only by the parallel component of the field to the given rhombohedral axis. Projecting the critical magnetic fields to the corresponding rhombohedral axes reveals the universal (single-domain) phase diagram with the magnetic field parallel to the easy axis [20].

(ii) The modulation vectors of the Cyc and SkL states are confined to the plane perpendicular to the rhombohedral axis in each structural variant irrespective of the direction of the applied magnetic field [20,30]. Therefore, the structural domain boundaries are necessarily boundaries to the consistent magnetic structures as well [27].

(iii) The phase transitions between the modulated states may be influenced by domain boundary effects. For instance, skyrmion formation mediated by grain boundaries has been observed in chiral magnets [6,32,33]. Moreover, the disorder induced by the structural domain boundaries could possibly lead to a spatial variation of the cycloidal wavelength and the SkL lattice constant.

The skyrmion lattice in GaV_4S_8 was demonstrated to carry magnetoelectric polarization [25,29], offering possibilities of skyrmion manipulation with external electric fields.

The measurement of static magnetization or magnetic susceptibility is a primary methodology to reveal the phase transitions between the modulated magnetic states in noncentrosymmetric magnets [9,20,34–36]. Beyond the determination of the phase diagram via dc susceptibility measurements, recently, several works have been devoted to analyzing the dynamic response of the modulated spin structures via ac susceptibility measurements. Similar features have been identified in the ac susceptibility in many compounds of the B20 family as well as in Cu_2OSeO_3 [34,37–41]. Generally, the real component of the ac susceptibility follows well the static susceptibility, however in the vicinity of the magnetic phase boundaries, it deviates from the static value and becomes strongly frequency dependent, accompanied with a finite imaginary component of the susceptibility. In chiral helimagnets, this feature is generally interpreted as the signature of slow relaxation processes of large correlated magnetic volumes, such as the reorientation of the long-wavelength spin spirals, propagation of topological defects, and the nucleation of skyrmionic cores, taking place upon the magnetic phase transitions [37,38,40,41]. The analysis of the frequency dependence of the ac susceptibility in all cases revealed a broad distribution of relaxation times at the phase boundaries, with values ranging up to the minutes scale [38,40,41].

Here, we report a systematic study of the ac susceptibility in GaV_4S_8, a compound essentially different from the cubic helimagnets in terms of crystal symmetries and magnetic phase diagram [20]. The analysis of the susceptibility measurements reveals a dramatic increase of the relaxation times in the vicinity of the magnetic phase boundaries, with a strong temperature dependence, which is similar to findings in other skyrmion-host systems [38,40,41]. The average relaxation times are much shorter than 1 ms at the high-temperature end of each phase boundary and rise well above the minute scale at the low-temperature limits. This strong temperature dependence suggests a thermally activated behavior of the relaxation processes characterized by energy barriers in the order of 1000 K, likely due to pinning of extended regions.

II. RELAXATION MODEL

The modulated magnetic structures in skyrmion host compounds are generally characterized by a long correlation length, forming coherent magnetic regions with dimensions of hundreds of nanometers [3,20]. The ac susceptibility of correlated spin structures consisting of clusters and/or domains of various volumes is generally described by the Cole-Cole relaxation model. This phenomenological model has been effectively applied to various systems [42] comprising large magnetic volumes, such as spin glasses [43], superparamagnetic nanoparticles [44], and more recently it has been proposed for the description of the relaxation processes at the phase transitions between modulated magnetic states in chiral helimagnets, $Fe_{1-x}Co_xSi$ [40] and Cu_2OSeO_3 [38,41].

The dynamic response of the magnetic system in the Cole-Cole model is formulated as an extension of the Debye relaxation by introducing a distribution of relaxation times, while keeping the exponential time dependence of the relaxation [42,45]:

$$\chi(\omega) = \chi_\infty + (\chi_0 - \chi_\infty)\frac{1}{1 + (i\omega\tau_c)^{1-\alpha}}, \tag{1}$$

where τ_c represents the central value of the relaxation times and the α parameter is connected to the width of their distribution. The response of the magnetic system is separated into two components according to their characteristic time scales as compared to the studied frequency range. The fast response of the spins occurring at frequencies much larger than our experimental window ($1/\tau \gg 1$ kHz) are referred to as adiabatic, approximated by a frequency-independent and purely real quantity χ_∞, in the frequency range covered by our study. The slow relaxation processes responsible for the frequency dependence of the susceptibility in the low-frequency range of the experiments is described by the second term in Eq. (1). The static limit of the ac susceptibility is denoted as χ_0. The distribution of the relaxation times, $g[\ln(\tau)]$, is expressed by the τ_c and α parameters as follows [45]:

$$g(\ln\tau) = \frac{1}{2\pi}\left(\frac{\sin\alpha\pi}{\cosh\left[(1-\alpha)\ln(\tau/\tau_c) - \cos\alpha\pi\right]}\right). \tag{2}$$

The distribution is symmetric on the logarithmic scale with the central value of τ_c. The zero value of α represents a single Debye-relaxation process, while values close to unity lead to an infinitely broad distribution of relaxation times.

Owing to the phase sensitivity of the ac-susceptibility measurements, both the real and imaginary components of the susceptibility, $\chi'(\omega)$ and $\chi''(\omega)$, can be recovered. The frequency dependence of the two components, expressed from Eq. (1), reads as

$$\chi'(\omega) = \chi_\infty + (\chi_0 - \chi_\infty)\frac{\omega\tau_c^{\alpha-1} + \sin\left(\frac{\alpha\pi}{2}\right)}{\omega\tau_c^{\alpha-1} + \omega\tau_c^{1-\alpha} + 2\sin\left(\frac{\alpha\pi}{2}\right)}, \tag{3}$$

$$\chi''(\omega) = (\chi_0 - \chi_\infty)\frac{\cos\left(\frac{\alpha\pi}{2}\right)}{\omega\tau_c^{\alpha-1} + \omega\tau_c^{1-\alpha} + 2\sin\left(\frac{\alpha\pi}{2}\right)}. \tag{4}$$

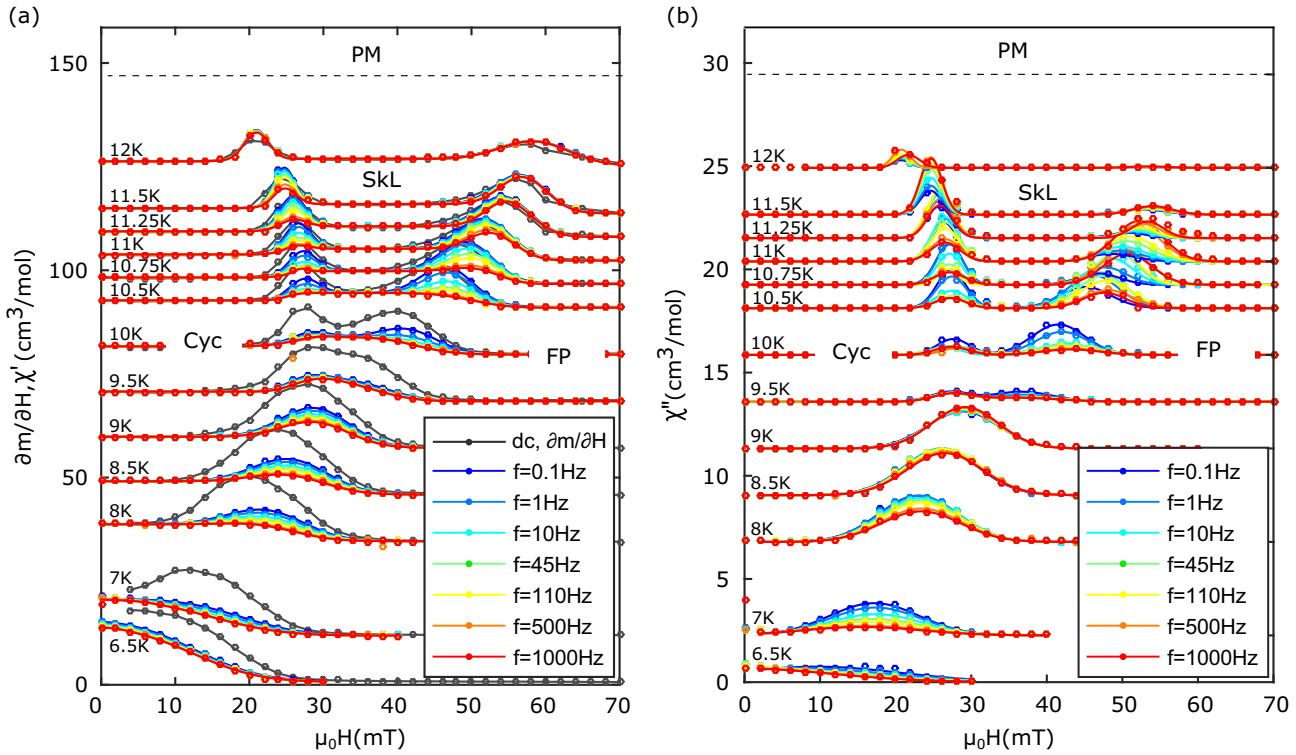

FIG. 1. Static and ac susceptibility measured in GaV_4S_8, plotted against the external magnetic field. Panel (a) presents the static susceptibility, $\partial m/\partial H$, plotted in gray, along with the real component of the ac susceptibility, $\chi'(H)$. Panel (b) displays the imaginary component of the ac susceptibility, $\chi''(H)$. Different colors represent data measured at various ac frequencies in the $f = 0.1$-Hz–1-kHz range. Measured data are shifted proportionally with the sample temperature, which is indicated on the left side of each curve. The continuous lines connecting the dots are guides to the eye. The magnetic phases separated by the susceptibility peaks in the B-T plane are indicated in the graphs. The paramagnetic state above $T_C = 13$ K is denoted as PM.

III. METHODS

A. Sample synthesis and characterization

Single crystalline GaV_4S_8 samples were grown by chemical vapor transport method using iodine as transport agent. The high crystalline quality of the samples has been confirmed by x-ray diffraction. A cuboid-shaped sample with a mass of 23.4 mg was selected for the ac susceptibility measurements.

B. Static and ac susceptibility measurements

A 5T Quantum Design MPMS superconducting quantum interference device magnetometer was used for the static and ac susceptibility measurements. Both the static magnetic field and the ac modulation field were normal to the (111) plane of the GaV_4S_8 crystal and the longitudinal magnetic moment was measured in a phase sensitive manner. The field dependence of the ac susceptibility was measured in the 0–80-mT range with a modulation amplitude of $\mu_0 H^\omega = 0.3$ mT. In order to probe the dynamics of the magnetically ordered spin system in the low-frequency regime, the drive frequency of the modulating coil was varied between $f = 0.1$ Hz and 1 kHz. The in-phase and out-of-phase components of the oscillating magnetization were measured and normalized by the drive amplitude H^ω to obtain the real and imaginary parts of the ac susceptibility, respectively. The dc magnetization was measured in a subsequent run after the ac susceptibility measurements. The static susceptibility $\partial m/\partial H$ was obtained from the measured dc magnetization curves by numerical derivation. The typical duration of the static measurements was $\approx$100 s per data point, which involved the ramping of the magnetic field and performing the measurement by the reciprocating sample option (RSO).

IV. RESULTS AND DISCUSSION

The magnetic-field dependence of the static and ac susceptibility was recorded at various temperatures within the magnetically ordered phases of GaV_4S_8, i.e., between $T = 6.5$ K and $T = 12$ K with magnetic fields applied parallel to the crystallographic $\langle 111 \rangle$ axis. The static susceptibility and the real part of the ac susceptibility are shown in Fig. 1(a). The imaginary component of the ac susceptibility is presented in Fig. 1(b).

A. Magnetic phase diagram established by static and ac susceptibility measurements

The field-driven phase transitions are associated with anomalies in the static susceptibility [20,34]. The susceptibility measurements presented in Fig. 1 reveal distinct peaks near the critical fields of the phase transitions between the Cyc, SkL, and FP states, following a clear temperature dependence, and resulting essentially in the same phase diagram as established by Kézsmárki *et al.* in earlier static magnetization

measurements [20]. The three states adjoin at the triple point located at $T = 9.5$ K and $\mu_0 H = 32$ mT.

Despite the coexistence of structural domains in the compound, within the studied field range, phase transitions are only observed in the unique structural variant wherein the rhombohedral axis is parallel to the field, i.e., points along the [111] axis. In the other three variants with their rhombohedral axes along $[\bar{1}\bar{1}1]$, $[\bar{1}1\bar{1}]$, and $[1\bar{1}\bar{1}]$ the Cyc phase persists up to fields higher than $\mu_0 H = 80$ mT [20], showing no anomalies in the studied field range.

The susceptibility peaks observed in Fig. 1 are not sharp but extend over relatively wide regions of magnetic fields. These regions are presumably characterized by the coexistence of the magnetic phases [34,37], as has been observed in various skyrmion host compounds in real space via magnetic force microscopy [46] and Lorentz-TEM imaging [4,6,10,47]. In the case of GaV_4S_8, the lamellar structure of the ferroelastic domains with a typical thickness in the micrometer range [27] may introduce significant disorder in the vicinity of domain boundaries and may also enhance demagnetizing fields in the sample. However, the relatively wide susceptibility peaks as compared to the values of the critical magnetic fields suggest that disorder is likely to play the key role in the broadening of phase transitions.

Figure 2(a) presents the dc magnetization along with the calculated static susceptibility ($\partial m/\partial H$) and the real part of the ac susceptibility measured with the highest modulation frequency, $f = 1$ kHz at $T = 11$ K, where all three magnetic phases are present. Magnetization measurements in increasing and decreasing fields did not reveal any hysteresis.

The pure Cyc, SkL, and FP phases are characterized by the static susceptibility values fully tracked by the ac susceptibility, even at 1 kHz. The frequency independence of the susceptibility in the phase-pure regions may be caused either by the vanishing of the low-frequency relaxation processes, i.e., $(\chi_0 - \chi_\infty) = 0$ in Eqs. (3) and (4), or by the increase of their characteristic frequency above the experimental window, $1/\tau_c \gg 1$ kHz. The former scenario is confirmed by fitting Eqs. (3) and (4) to the experimental data, as discussed in Sec. IV C. Therefore, the measured static susceptibility in the pure phases corresponds to the adiabatic values, as $\chi_0 = \chi_\infty$. Remarkably, the susceptibility is enhanced in the SkL phase as compared to the Cyc phase, in contrast to the B20 compounds, where the SkL phase is typically seen as a dip in the susceptibility of the embedding conical state [34]. In this longitudinal conical state, the magnetic field is roughly perpendicular to the rotation plane of the spins, while in the present case the magnetic field is applied within the spin rotation plane of the cycloids. Correspondingly, a lower susceptibility is expected in the latter case. The inset of Fig. 2(b) shows the values of the susceptibility as a function of the temperature in the magnetic field regions of the pure Cyc and SkL phases, as indicated by black arrows in Fig. 2(a) at $T = 11$ K. The adiabatic susceptibility increases towards lower temperatures, but remains larger in the SkL phase than in the Cyc phase at all temperatures. In the FP state the susceptibility is nearly zero, with contributions from the persisting Cyc phase in the three nonunique domains and the unsaturated moments in the FP state in the unique domain.

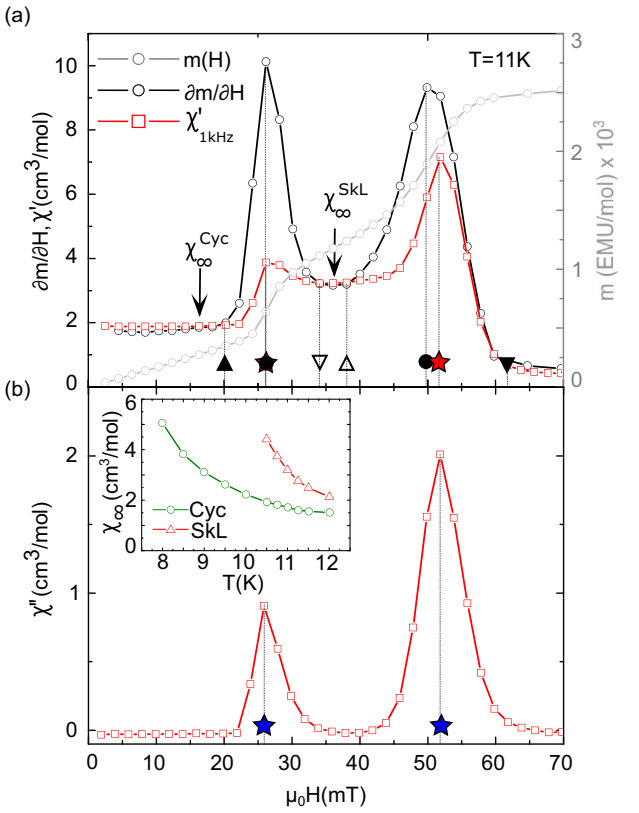

FIG. 2. Panel (a) shows the magnetization curve $m(H)$ (right axis, gray curve), along with the static susceptibility $\partial m/\partial H$ and the ac susceptibility data measured with the highest modulation frequency, $f = 1$ kHz at $T = 11$ K (left axis, black and red curves, respectively). Panel (b) displays the imaginary component of the ac susceptibility at the same temperature and modulation frequency. The inset compares the adiabatic susceptibility, χ_∞ in the Cyc and SkL phases at various temperatures, obtained from the dc susceptibility curves as indicated by the black arrows in panel (a). The symbols signaling the main features of the susceptibility curves are the same as those used in Fig. 3.

Figure 2(b) displays the imaginary component of the ac susceptibility, measured at 11 K with $f = 1$ kHz modulation frequency. The two peaks located at the Cyc-SkL and SkL-FP phase transitions are attributed to dissipative processes occurring at low frequencies, which will be discussed in detail in Sec. IV B.

We construct the magnetic phase diagram, presented in Fig. 3, relying on the main features of the static and ac susceptibility data measured with the highest modulation frequency, $f = 1$ kHz.

The phase diagram displays the main features of the susceptibility curves, as indicated in Fig. 2 using the same symbols: $B_c^{\mathrm{Cyc}}(+)$ and $B_c^{\mathrm{SkL}}(+)$ correspond to the higher-field boundaries of the phase pure Cyc and SkL phases, respectively, while $B_c^{\mathrm{SkL}}(-)$ and $B_c^{\mathrm{FP}}(-)$ are the lower-field boundaries of the pure SkL and FP phases, respectively. The position of the maximum values in the static susceptibility, associated with the critical fields of the phase transitions in previous studies [20,25,29], are also indicated in the phase diagram, along with the location of the peaks in the real and imaginary components

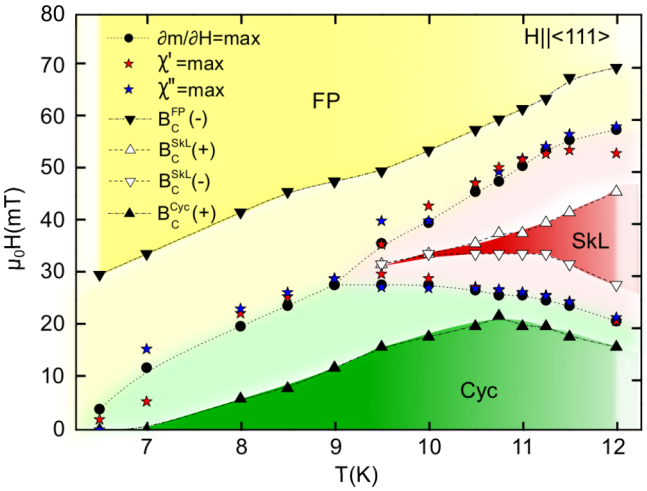

FIG. 3. Magnetic phase diagram of GaV_4S_8 established by static magnetization and ac susceptibility measured at $f = 1$ kHz. Upward and downward pointing triangles represent the beginning and the end of the peaks in the static susceptibility, separating the pure Cyc, SkL, and FP phases from the regions of phase coexistence, indicated by pale shadowing. Full circles represent the location of the peaks in the static susceptibility, associated to the phase boundaries in earlier reports [20,25,29]. Red and blue stars display the location of the maxima in the real and imaginary parts of the ac susceptibility using a modulation frequency of 1 kHz.

of the ac susceptibility. The critical fields determined from the ac susceptibility curves agree well with those obtained from the static susceptibility, however the position of the ac susceptibility peaks is clearly frequency dependent—see, e.g., the susceptibility curves measured at $T = 10.5$ K in Fig. 1(b).

B. Slow relaxation phenomena at the magnetic phase boundaries

It is clearly seen in Figs. 1(a) and 1(b) that away from the phase transitions, the ac susceptibility is frequency independent and purely real, with values identical to the static susceptibility. In these regions, the characteristic relaxation times are much shorter than 1 ms, the time period of the highest-frequency modulation in our experiments, i.e., the measured frequency-independent susceptibility values correspond to χ_∞. On the other hand, in the field range of the phase transitions, the real component of the ac susceptibility falls behind the static values, accompanied with a peak in the imaginary component, both exhibiting strong frequency dependence. These features indicate extremely slow relaxation processes with characteristic frequencies close to, or below the range of $f = 0.1$–1000 Hz, used in the experiment. Such behavior was also reported in cubic helimagnets of the B20 family [35,37,40,48] and in Cu_2OSeO_3 [38,41] in the vicinity of the magnetic phase transitions. The dynamics governing the Cyc-SkL phase transition is expected to be rather similar to the conical-SkL transition observed in chiral magnets. There, the phase coexistence region is characterized by the nucleation of the skyrmions through the emergence of topological point defects, monopoles, and antimonopoles, as the helical states are unzipped [4,46]. The excitation of these defects over pinning barriers might lead to the observed frequency dependence of the susceptibility [38]. Moreover, the emerging SkL, coexisting with the helical states is prone to develop lattice defects such as irregular coordination or edge dislocations, eventually relaxing to the equilibrium single domain SkL state in the pure SkL phase [4,47]. The ac-field-induced relaxation of the defects in the SkL may also be responsible for the slow dynamics seen in the ac susceptibility measurements.

However, due to the absence of the longitudinal conical state in GaV_4S_8, the Cyc-FP and the SkL-FP transitions are unique in this material, featuring different dynamical processes than those present in the cubic helimagnets, which is also reflected in the real and imaginary susceptibility components at the phase transitions. Below, we discuss the main differences between the ac magnetic response of the two types of materials:

(i) In cubic helimagnets the zero-field multidomain helical state is rearranged by the external magnetic field and a longitudinal conical state with the modulation vector parallel to the field is established [9,10,34,37,49–52]. ac susceptibility measurements in FeGe [48], MnSi [37,52], Cu_2OSeO_3 [38,41], and $Fe_{1-x}Co_xSi$ [40] revealed a frequency-dependent peak in the susceptibility accompanied with a finite dissipation emerging over this transition. These features of the ac susceptibility indicate that the rearrangement of the large magnetic spirals occurs on extended time scales.

In GaV_4S_8, on the other hand, the zero-field state is cycloidal with the modulation vectors confined to the plane perpendicular to the rhombohedral axis in each domain [20]. As demonstrated by recent SANS measurements [30], the q vectors are distributed evenly over rings within the ⟨111⟩-type planes, indicating a negligible (or weak) in-plane anisotropy. The external field applied in the [111] direction does not break the isotropy of the (111) plane, therefore the modulation directions in the unique domain remain unaffected by the field, which is in accord with the absence of dissipation within the pure Cyc phase.

(ii) In the bulk chiral magnets, the FP state is achieved through the longitudinal conical state by the continuous closing of the conical angle [34]. The fact that ac susceptibility measurements do not reveal dissipation and frequency-dependent susceptibility at the conical-FP phase boundary [34] indicates that this process occurs on time scales much faster than those of the ac modulations.

Oppositely, in GaV_4S_8, the FP state is achieved by the expansion of the cycloidal pitch and the increasing anharmonicity of the modulation [49], similarly to monoaxial chiral magnets [53]. In addition, structural disorder may introduce pinning along with a spatial variation of the modulation wavelength. According to earlier SANS measurements, the modulation wavelength indeed shows significant increase in the vicinity of the FP state [20]. Recent SANS measurements reveal strong fluctuations in the cycloidal wavelength along the temperature-driven phase transition from the Cyc to the zero-field ferromagnetic state below 6 K, supporting this scenario [30].

The spatial variation in the length or orientation of the cycloidal wave vector is expected to result in the formation of topological defects, such as edge disclinations [4,6,52,54]. The slow relaxation observed in the ac susceptibility measurements at the Cyc-FP boundary are probably associated to the

field-induced motion of such defects along the phase fronts of the spin cycloids, involving the collective excitation of a large number of spins over pinning barriers.

(iii) A phase coexistence between the SkL and the FP states has been observed in thin films of cubic helimagnets, where the conical state is suppressed by the geometrical confinement [4]. In elevated magnetic fields a glassy state of skyrmions is realized, exhibiting large fluctuations in the SkL orientation and lattice constant [4,55]. Relaxation processes involving the rearrangement of such SkL clusters may govern the slow dynamics at the SkL-FP phase transition in GaV_4S_8.

C. Temperature and magnetic-field dependence of the relaxation processes

The frequency dependence of the peaks in both susceptibility components [Figs. 1(a) and 1(b)] shows a strong variation with the temperature. Concerning the Cyc-FP phase boundary, at $T = 7$ K the dissipation is the largest for the smallest modulation frequency, whereas at $T = 9$ K it becomes almost frequency independent. Above the triple point between $T = 10$ K and $T = 11$ K, a reversal can be seen in the hierarchy of the frequencies in the dissipation peaks at both the Cyc-SkL and SkL-FP phase boundaries, indicating that the characteristic frequencies of the relaxation processes pass through the measurement window. Additionally, the peaks in the imaginary part of the susceptibility are shifted in magnetic field with the change of the drive frequency, which is most prominent at $T = 10.5$ K. In order to systematically investigate the behavior of the relaxation as the function of the temperature and magnetic field, the frequency dependence of the real and imaginary components of the susceptibility was analyzed at all measured (H,T) points in the vicinity of the magnetic phase boundaries.

Figure 4 shows the frequency dependence of χ' and χ'' in various magnetic fields. Three representative temperatures are selected above the triple point, where the peak in the imaginary part of the susceptibility passes through the experimental window, indicating that the inverse relaxation times go through the range of the measurement frequencies. Figure 4 shows only the data measured in representative magnetic field regions near the Cyc-SkL and SkL-FP phase transitions. The frequency dependence of the complex susceptibility can be fitted well by the Cole-Cole relaxation model [Eqs. (3) and (4)] using the same set of parameters for the real and imaginary components. The shifting of the peak in χ'' towards lower frequencies with decreasing temperature is well traced by the fitted curves for both the Cyc-SkL and the SkL-FP transitions implying an overall slowing down of the relaxation.

Figure 5(a) presents the fitted magnitudes $(\chi_0 - \chi_\infty)$ of the low-frequency relaxation processes at all temperatures as a function of the magnetic field. According to the fitting, the magnitude of these processes vanishes smoothly in the vicinity of the pure phases, while the associated relaxation time scales remain accessible by our measurements [as seen, e.g., in Figs. 4(b), 4(d) and 4(f)]. This indicates that the slow relaxation phenomena arise only in the range of the phase coexistence, and the magnitude of the frequency-dependent

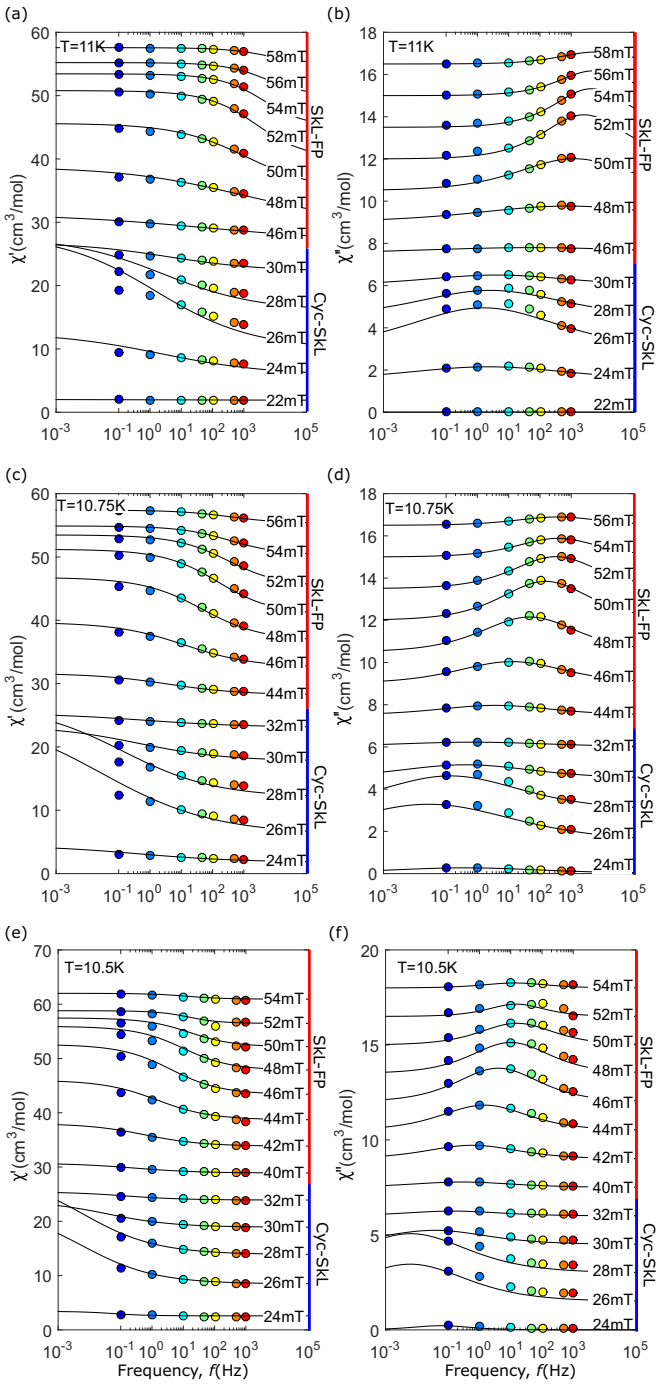

FIG. 4. Frequency dependence of the real (left column) and imaginary components (right column) of the susceptibility in various magnetic fields above the temperature of the triple point, at $T = 11$ K (top), $T = 10.75$ K (middle), and $T = 10.5$ K (bottom row). Measured values are shifted with respect to the magnetic field. The color coding of the measured values represents the different ac frequencies in accordance with Fig. 1. Solid lines are fitted curves according to Eqs. (3) and (4) with the same set of parameters for the real and imaginary parts of the susceptibility. The blue and red bars next to the right axes represent the range of magnetic fields corresponding to the Cyc-SkL and SkL-FP phase transitions, respectively.

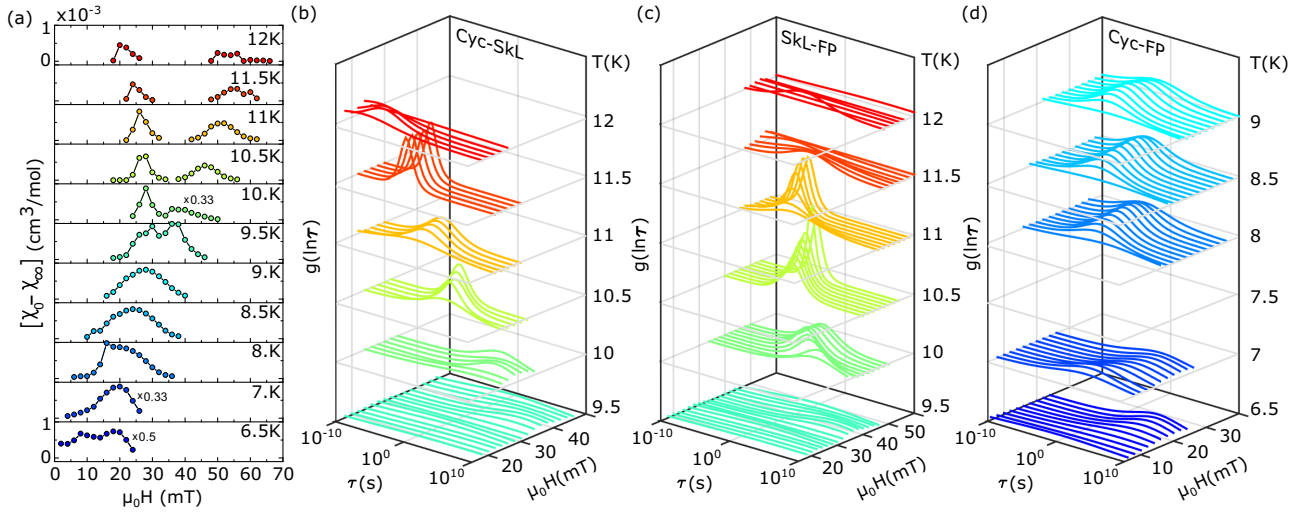

FIG. 5. Panel (a) shows the fitted magnitude of the low-frequency susceptibility, $(\chi_0 - \chi_\infty)$, as a function of the magnetic field at various temperatures. The fitted values are scaled to a common range using the factors indicated at three temperatures. Panels (b)–(d) present the distribution of relaxation times, $g[\ln(\tau)]$, plotted as a function of the temperature and magnetic field. The distributions were calculated employing Eq. (2) with the τ_c and α parameters obtained from the fits to the frequency dependence of the complex susceptibility. Panels (b)–(d) present the relaxation times in the ranges of magnetic fields corresponding to the Cyc-SkL, SkL-FP, and Cyc-FP transitions, respectively. The distribution curves are shifted proportionally with the temperature along the z axis, which is also indicated in the right side of the graphs. The curves are colored according to a color map representing decreasing temperatures ranging from $T = 12$ K (red) to $T = 6.5$ K (blue). The average relaxation time shows a dramatic decrease with decreasing temperatures along all the three phase boundaries, with values well above 10 s at their low-temperature limits.

susceptibility is probably connected to the density of magnetic defects, vanishing in the pure phases. It further confirms, that the frequency-independent susceptibility measured inside the pure phases can be regarded as adiabatic, $\chi_0 = \chi_\infty$, as previously assumed in Fig. 2.

Using the τ_c and α parameters retrieved from the Cole-Cole fits, the distribution of the relaxation times $g(\ln\tau)$ was calculated for each (H,T) point, according to Eq. (2). Figures 5(b)–5(d) display the calculated distributions of the relaxation times for the Cyc-SkL, SkL-FP, and Cyc-FP phase transitions, respectively. For each transition, the characteristic time scales fall below $\tau \ll 1$ ms at the high-temperature end of the phase boundary, exhibiting a dramatic increase towards lower temperatures, reaching values $\tau \gg 10$ s at the low-temperature part of the phase boundaries. Similar tendencies have been identified in Cu_2OSeO_3 [38,41].

Figure 6 presents the temperature dependence of the fitted relaxation times averaged over the range of magnetic fields near the phase transitions as $\ln(\tau_{av}) = \sum_i^N \ln[\tau(H_i)]/N$. The sum runs over the values of relaxation times, $\tau(H_i)$, which are determined by fitting at each field H_i, where the susceptibility shows observable frequency dependence in the vicinity of the phase boundaries. The error bars assigned to the data are calculated as the standard deviation of the $\ln[\tau(H_i)]$ values. The rapid drop in the relaxation times with increasing temperatures is clearly seen for each phase boundary. The discontinuous jump in the relaxation time at the triple point marks an abrupt change in the relaxation processes between the Cyc-FP and the Cyc-SkL phase.

The exponential character of the temperature dependence of the relaxation times suggests a thermally activated behavior possibly related to the pinning barriers of the topological defects, ΔE. The energy barriers over the Cyc-SkL and SkL-FP phase transitions were estimated by linear fits to the Arrhenius plots, i.e., $\ln(\tau_{av})$ against $1/T$, as presented in the inset of Fig. 6. The fitted values yield average activation energies of 1300 K $\pm$150 K and 1100 K $\pm$35 K at the Cyc-SkL and the SkL-FP boundaries, respectively, where the values of the uncertainty are estimated from the linear fits, taking the error bars of the data points into consideration. These large values imply the reorientation dynamics of sizable magnetic regions instead of individual spins. Since the susceptibility at the Cyc-FP boundary could not be accurately fitted (as discussed later), the relaxation times for this transition have not been analyzed quantitatively.

In contrast to the other two phase boundaries, the Cole-Cole model fails to fit the frequency dependence of the complex susceptibility for the Cyc-FP transition, as demonstrated in Fig. 7 for two selected temperatures below the triple point. Even though the real and the imaginary components can be fitted separately with two different sets of parameters (see dashed gray curves in Fig. 7), the resulting parameters convey no physical meaning, as the Kramers-Kronig relation does not hold between the two components of the response function. The large difference between the static susceptibility values and the real part of the ac susceptibility measured even at the lowest frequency of $f = 0.1$ Hz, as seen in Fig. 1(a), suggests that dynamic processes exist with characteristic relaxation times far beyond 10 s.

The Cole-Cole model assumes a symmetric distribution of relaxation times on the logarithmic scale [45], which may not apply for more complex processes involved in the

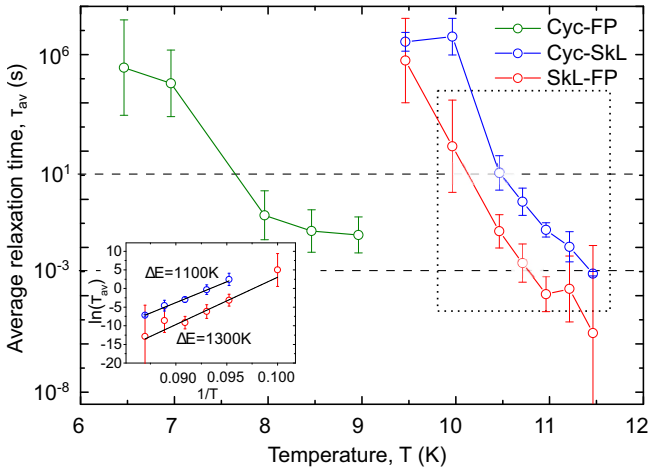

FIG. 6. Temperature dependence of the logarithmic average of the relaxation times obtained from the Cole-Cole fits, where the averaging was performed over the fitted values in the magnetic field region close to the phase transitions. The green, red, and blue circles correspond to the average relaxation times at the Cyc-FP, Cyc-SkL, and SkL-FP transitions. The error bars represent the standard deviation of the relaxation times on the logarithmic scale. The lines connecting the data points are guides to the eye. The dashed horizontal lines represent the measurement window defined by the inverse of the highest (1 kHz) and lowest (0.1 Hz) ac frequencies. The inset presents $\ln \tau_{av}$ as the function of $1/T$ along the Cyc-SkL and SkL-FP phase boundaries. Relaxation time values close to the experimental window are plotted, as indicated by the black dotted frame. Linear fits to the data (solid black lines) yield the approximate average activation energies of 1100 and 1300 K near the Cyc-SkL and SkL-FP phase boundaries, respectively.

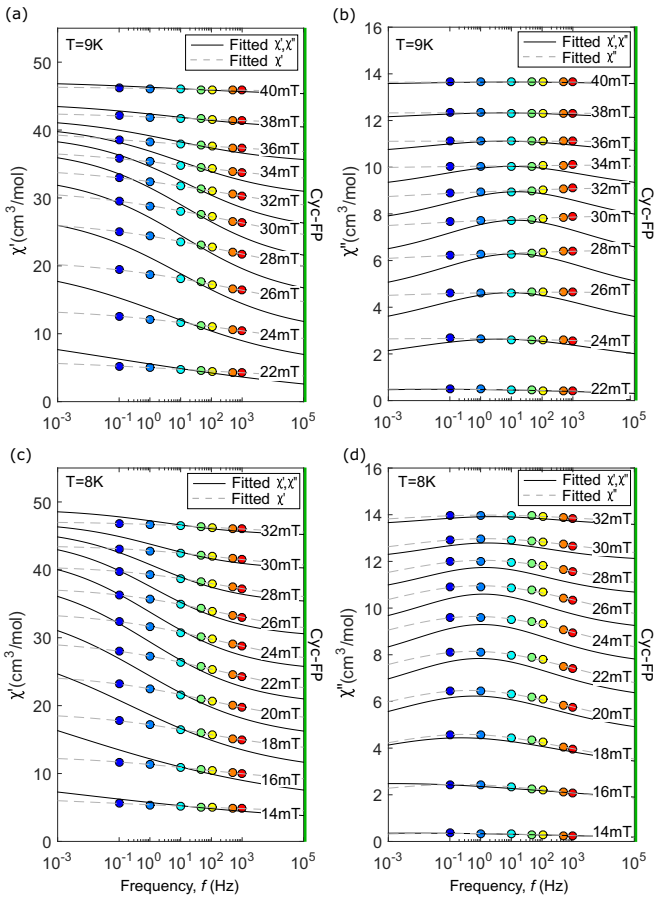

FIG. 7. Frequency dependence of the real (left column) and imaginary components (right column) of the susceptibility in various magnetic fields below the temperature of the triple point at T = 9 K (top), T = 8 K (bottom row). Measured values are shifted with respect to the magnetic field. The color coding of the measured values represents the different ac frequencies in accordance with Fig. 1. Solid lines are fitted curves according to Eqs. (3) and (4) with the same set of parameters for the real and imaginary parts of the susceptibility. Gray dashed lines are separate fits to the real [(a) and (c)] and the imaginary components [(b) and (d)] of the susceptibility. The green bars next to the right axes emphasize that the range of magnetic fields at the given temperatures correspond to the Cyc-FP phase transition.

magnetic phase transitions in GaV_4S_8. A generalization of the Cole-Cole function was provided by Havriliak and Negami [56] allowing for an asymmetric distribution of relaxation times [57]. Applying the Havriliak-Negami model to our data, however, yielded the same parameters as the Cole-Cole fits returning the same symmetric distribution of relaxation times, and hence did not improve the fit.

Only a few recent studies made an attempt to quantitatively describe the relaxation processes at the magnetic phase boundaries in cubic skyrmion host compounds, each within the framework of the Cole-Cole model [38,40,41]. However, in most of these studies the real and imaginary components of the ac susceptibility were handled separately, which may lead to unphysical parameters, as seen for the Cyc-FP transition in GaV_4S_8 (Fig. 7). Qian *et al.* correlated the Cole-Cole fits to the real and the imaginary parts of the susceptibility in Cu_2OSeO_3, finding good agreement in case of the conical-to-skyrmion and skyrmion-to-conical transitions, whereas a discrepancy was reported at the helical-to-conical transition. The authors attributed this difference to additional relaxation processes present at extremely low frequencies. Bannenberg *et al.* [40] also identified a low-frequency contribution to the dissipation in $Fe_{1-x}Co_xSi$ that could not be described by the Cole-Cole model both at the conical-to-skyrmion and the skyrmion-to-conical transitions.

V. CONCLUSION

In this study, we investigated the dynamics of the field-driven phase transitions between the magnetic states in GaV_4S_8 via ac susceptibility measurements. The magnetic structures within the pure Cyc, SkL, and FP phases are characterized by an instantaneous response to the ac modulation, i.e., on frequency scales well above the kHz range. The emergence of extremely slow dynamics was observed at the phase boundaries between the cycloidal, skyrmion lattice, and field-polarized states.

Similar frequency-dependent susceptibility and peaks in the imaginary (dissipative) part of the susceptibility characterize the phase boundaries between modulated magnetic states in all cubic helimagnets [34]. In comparison with cubic helimagnets, we discussed the fundamental differences in the phase transitions due to the absence of the longitudinal

conical state in GaV_4S_8, resulting in the direct transition from the Cyc and SkL phases to the FP state. Remarkably, these transitions are also characterized by low-frequency relaxation processes, suggesting the involvement of large magnetic volumes, possibly related to the topological defects created in the course of the phase transition.

The magnetization dynamics at the Cyc-SkL and SkL-FP phase transitions in GaV_4S_8 is well described by the Cole-Cole relaxation model. However, discrepancies found at the Cyc-FP transition indicate a more complex behavior that cannot be described by a distribution of Debye-relaxation processes.

Each field-driven phase transition in GaV_4S_8 shows similar behavior as a function of the temperature: at the high-temperature end of the phase boundaries the characteristic relaxation times are much shorter than 1 ms, whereas at the lower-temperature part of the phase boundaries, the dynamics is drastically slowed down, characterized by relaxation times well above the minute scale. Similar temperature dependence of the relaxation times has been reported for Cu_2OSeO_3 [38,41] and may be a common feature for all bulk skyrmion host materials. The broad distribution of relaxation times and their strong dependence on the temperature, implying large activation energies, are likely the results of the collective relaxation of large magnetic structures of various volumes. The similarities and differences identified between the ac magnetic response of GaV_4S_8 and the chiral helimagnets may provide further hints and motivate a more complete understanding of the complex dynamics emerging near the magnetic phase transitions in the skyrmion host materials.

ACKNOWLEDGMENTS

The authors thank I. Živković and H. M. Rønnow for enlighting discussions. This work was supported by the Deutsche Forschungsgemeinschaft through the Transregional Collaborative Research Center TRR 80 and by the Hungarian Research Funds OTKA K 108918, OTKA PD 111756 and Bolyai 00565/14/11.

[1] A. Bogdanov and D. Yablonskii, Zh. Eksp. Teor. Fiz. **95**, 178 (1989) [JETP **68**, 101 (1989)].
[2] N. Nagaosa and Y. Tokura, Nat. Nanotechnol. **8**, 899 (2013).
[3] S. Mühlbauer, B. Binz, F. Jonietz, C. Pfleiderer, A. Rosch, A. Neubauer, R. Georgii, and P. Böni, Science **323**, 915 (2009).
[4] X. Yu, Y. Onose, N. Kanazawa, J. Park, J. Han, Y. Matsui, N. Nagaosa, and Y. Tokura, Nature (London) **465**, 901 (2010).
[5] M. Uchida, N. Nagaosa, J. P. He, Y. Kaneko, S. Iguchi, Y. Matsui, and Y. Tokura, Phys. Rev. B **77**, 184402 (2008).
[6] X. Yu, N. Kanazawa, Y. Onose, K. Kimoto, W. Zhang, S. Ishiwata, Y. Matsui, and Y. Tokura, Nat. Mater. **10**, 106 (2011).
[7] K. Shibata, X. Yu, T. Hara, D. Morikawa, N. Kanazawa, K. Kimoto, S. Ishiwata, Y. Matsui, and Y. Tokura, Nat. Nanotechnol. **8**, 723 (2013).
[8] G. Meunier and M. Bertaud, J. Appl. Crystallogr. **9**, 364 (1976).
[9] T. Adams, A. Chacon, M. Wagner, A. Bauer, G. Brandl, B. Pedersen, H. Berger, P. Lemmens, and C. Pfleiderer, Phys. Rev. Lett. **108**, 237204 (2012).
[10] S. Seki, X. Yu, S. Ishiwata, and Y. Tokura, Science **336**, 198 (2012).
[11] J. S. White, I. Levatić, A. Omrani, N. Egetenmeyer, K. Prša, I. Živković, J. Gavilano, J. Kohlbrecher, M. Bartkowiak, H. Berger *et al.*, J. Phys.: Condens. Matter **24**, 432201 (2012).
[12] S. Seki, S. Ishiwata, and Y. Tokura, Phys. Rev. B **86**, 060403 (2012).
[13] J. White, K. Prša, P. Huang, A. Omrani, I. Živković, M. Bartkowiak, H. Berger, A. Magrez, J. Gavilano, G. Nagy *et al.*, Phys. Rev. Lett. **113**, 107203 (2014).
[14] Y.-H. Liu, Y.-Q. Li, and J. H. Han, Phys. Rev. B **87**, 100402 (2013).
[15] F. Jonietz, S. Mühlbauer, C. Pfleiderer, A. Neubauer, W. Münzer, A. Bauer, T. Adams, R. Georgii, P. Böni, R. Duine *et al.*, Science **330**, 1648 (2010).
[16] A. Fert, V. Cros, and J. Sampaio, Nat. Nanotechnol. **8**, 152 (2013).
[17] W. Koshibae, Y. Kaneko, J. Iwasaki, M. Kawasaki, Y. Tokura, and N. Nagaosa, Jpn. J. Appl. Phys. **54**, 053001 (2015).
[18] X. Zhang, M. Ezawa, and Y. Zhou, Sci. Rep. **5**, 9400 (2015).
[19] X. Zhang, G. Zhao, H. Fangohr, J. P. Liu, W. Xia, J. Xia, and F. Morvan, Sci. Rep. **5**, 7643 (2015).
[20] I. Kézsmárki, S. Bordács, P. Milde, E. Neuber, L. Eng, J. White, H. Rønnow, C. Dewhurst, M. Mochizuki, K. Yanai *et al.*, Nat. Mater. **14**, 1116 (2015).
[21] R. Pocha, D. Johrendt, and R. Pöttgen, Chem. Mater. **12**, 2882 (2000).
[22] H. Müller, W. Kockelmann, and D. Johrendt, Chem. Mater. **18**, 2174 (2006).
[23] Z. Wang, E. Ruff, M. Schmidt, V. Tsurkan, I. Kézsmárki, P. Lunkenheimer, and A. Loidl, Phys. Rev. Lett. **115**, 207601 (2015).
[24] J. Hlinka, F. Borodavka, I. Rafalovskyi, Z. Docekalova, J. Pokorny, I. Gregora, V. Tsurkan, H. Nakamura, F. Mayr, C. A. Kuntscher, A. Loidl, S. Bordács, D. Szaller, H.-J. Lee, J. H. Lee, and I. Kézsmárki, Phys. Rev. B **94**, 060104 (2016).
[25] E. Ruff, S. Widmann, P. Lunkenheimer, V. Tsurkan, S. Bordács, I. Kézsmárki, and A. Loidl, Sci. Adv. **1**, e1500916 (2015).
[26] K. Xu and H. J. Xiang, Phys. Rev. B **92**, 121112(R) (2015).
[27] Á. Butykai, S. Bordács, I. Kézsmárki, V. Tsurkan, A. Loidl, J. Döring, S. C. Kehr, P. Milde, E. Neuber, and L. M. Eng, Sci. Rep. **7**, 44663 (2017).
[28] C. Yadav, A. Nigam, and A. Rastogi, Phys. B (Amsterdam, Neth.) **403**, 1474 (2008).
[29] S. Widmann, E. Ruff, A. Günther, H.-A. Krug von Nidda, P. Lunkenheimer, V. Tsurkan, S. Bordács, I. Kézsmárki, and A. Loidl, Philos. Mag., 1 (2016), doi:10.1080/14786435.2016.1253885.
[30] J. S. White, Á. Butykai, R. Cubitt, D. Honecker, C. D. Dewhurst, L. F. Kiss, V. Tsurkan, and S. Bordács, arXiv:1704.03621.
[31] D. Ehlers, I. Stasinopoulos, I. Kézsmárki, T. Fehér, V. Tsurkan, H. K. von Nidda, D. Grundler, and A. Loidl, J. Phys.: Condens. Matter **29**, 065803 (2016).
[32] T. Matsumoto, Y.-G. So, Y. Kohno, H. Sawada, Y. Ikuhara, and N. Shibata, Sci. Adv. **2**, e1501280 (2016).
[33] Z.-A. Li, F. Zheng, A. H. Tavabi, J. Caron, C. Jin, H. Du, A. Kovács, M. Tian, M. Farle, and R. E. Dunin-Borkowski, Nano Lett. **17**, 1395 (2017).

[34] A. Bauer and C. Pfleiderer, in *Topological Structures in Ferroic Materials* (Springer, Cham, 2016), pp. 1–28.
[35] A. Bauer, A. Neubauer, C. Franz, W. Münzer, M. Garst, and C. Pfleiderer, Phys. Rev. B **82**, 064404 (2010).
[36] H. Nakamura, R. Ikeno, G. Motoyama, T. Kohara, Y. Kajinami, and Y. Tabata, J. Phys.: Conf. Ser. **145**, 012077 (2009).
[37] A. Bauer and C. Pfleiderer, Phys. Rev. B **85**, 214418 (2012).
[38] I. Levatić, V. Šurija, H. Berger, and I. Živković, Phys. Rev. B **90**, 224412 (2014).
[39] T. Ou-Yang, G. Shu, C. Hu, and F. Chou, J. Appl. Phys. **117**, 123903 (2015).
[40] L. J. Bannenberg, A. J. E. Lefering, K. Kakurai, Y. Onose, Y. Endoh, Y. Tokura, and C. Pappas, Phys. Rev. B **94**, 134433 (2016).
[41] F. Qian, H. Wilhelm, A. Aqeel, T. T. M. Palstra, A. J. E. Lefering, E. H. Brück, and C. Pappas, Phys. Rev. B **94**, 064418 (2016).
[42] M. Bałanda, Acta. Phys. Pol. A **124**, 964 (2013).
[43] C. A. M. Mulder, A. J. van Duyneveldt, and J. A. Mydosh, Phys. Rev. B **23**, 1384 (1981).
[44] F. Luis, E. del Barco, J. M. Hernández, E. Remiro, J. Bartolomé, and J. Tejada, Phys. Rev. B **59**, 11837 (1999).
[45] D. Huser, A. van Duyneveldt, G. Nieuwenhuys, and J. Mydosh, J. Phys. C **19**, 3697 (1986).
[46] P. Milde, D. Köhler, J. Seidel, L. Eng, A. Bauer, A. Chacon, J. Kindervater, S. Mühlbauer, C. Pfleiderer, S. Buhrandt *et al.*, Science **340**, 1076 (2013).
[47] J. Rajeswari, P. Huang, G. F. Mancini, Y. Murooka, T. Latychevskaia, D. McGrouther, M. Cantoni, E. Baldini, J. S. White, A. Magrez *et al.*, Proc. Natl. Acad. Sci. USA **112**, 14212 (2015).
[48] H. Wilhelm, M. Baenitz, M. Schmidt, C. Naylor, R. Lortz, U. Rößler, A. Leonov, and A. Bogdanov, J. Phys.: Condens. Matter **24**, 294204 (2012).
[49] Y. Ishikawa, K. Tajima, D. Bloch, and M. Roth, Solid State Commun. **19**, 525 (1976).
[50] P. Bak and M. H. Jensen, J. Phys. C **13**, L881 (1980).
[51] B. Lebech, J. Bernhard, and T. Freltoft, J. Phys.: Condens. Matter **1**, 6105 (1989).
[52] A. Bauer, A. Chacon, M. Wagner, M. Halder, R. Georgii, A. Rosch, C. Pfleiderer, and M. Garst, Phys. Rev. B **95**, 024429 (2017).
[53] Y. Togawa, T. Koyama, K. Takayanagi, S. Mori, Y. Kousaka, J. Akimitsu, S. Nishihara, K. Inoue, A. Ovchinnikov, and J.-i. Kishine, Phys. Rev. Lett. **108**, 107202 (2012).
[54] M. Uchida, Y. Onose, Y. Matsui, and Y. Tokura, Science **311**, 359 (2006).
[55] X. Yu, A. Kikkawa, D. Morikawa, K. Shibata, Y. Tokunaga, Y. Taguchi, and Y. Tokura, Phys. Rev. B **91**, 054411 (2015).
[56] S. Havriliak and S. Negami, J. Polym. Sci., Part C: Polym. Symp. **14**, 99 (1966).
[57] R. Zorn, J. Polym. Sci. Pol. Phys. **37**, 1043 (1999).